JEM

Article

BACE1 deletion in the adult mouse reverses preformed amyloid deposition and improves cognitive functions

Xiangyou Hu, Brati Das, Hailong Hou, Wanxia He, and Riqiang Yan

Department of Neurosciences, Lerner Research Institute, Cleveland Clinic, Cleveland, OH

BACE1 initiates the generation of the β-amyloid peptide, which likely causes Alzheimer's disease (AD) when accumulated abnormally. BACE1 inhibitory drugs are currently being developed to treat AD patients. To mimic BACE1 inhibition in adults, we generated BACE1 conditional knockout (BACE1$^{fl/fl}$) mice and bred BACE1$^{fl/fl}$ mice with ubiquitin-Cre^{ER} mice to induce deletion of BACE1 after passing early developmental stages. Strikingly, sequential and increased deletion of BACE1 in an adult AD mouse model (5xFAD) was capable of completely reversing amyloid deposition. This reversal in amyloid deposition also resulted in significant improvement in gliosis and neuritic dystrophy. Moreover, synaptic functions, as determined by long-term potentiation and contextual fear conditioning experiments, were significantly improved, correlating with the reversal of amyloid plaques. Our results demonstrate that sustained and increasing BACE1 inhibition in adults can reverse amyloid deposition in an AD mouse model, and this observation will help to provide guidance for the proper use of BACE1 inhibitors in human patients.

Journal of Experimental Medicine

INTRODUCTION

Alzheimer's disease (AD), which is the most common age-dependent neurodegenerative disease, is characterized by the presence of amyloid deposition, neurofibrillary tangles, progressive loss of synapses, and severe cognitive dysfunction (Braak and Braak, 1997; Corriveau et al., 2017). Excessive accumulation of β-amyloid peptides (Aβ) is a widely recognized early event that leads to the development of AD pathologies, including impairments in synaptic functions at various sites (Malenka and Malinow, 2011; Selkoe and Hardy, 2016; Yan et al., 2016). Generation of Aβ requires β-secretase, also called β-site amyloid precursor protein (APP)–cleaving enzyme 1 (BACE1), which cleaves APP to release a soluble N-terminal fragment and a membrane-anchored C-terminal fragment (Hussain et al., 1999; Sinha et al., 1999; Vassar et al., 1999; Yan et al., 1999; Lin et al., 2000). Further cleavage of the C-terminal fragment by γ-secretase excises Aβ (Sisodia and St George-Hyslop, 2002; De Strooper et al., 2012). Genetic mutations such as the K670M671 to N670L671 mutation (Mullan et al., 1992) or the A673 to T673 mutation (Jonsson et al., 2012) can either increase or decrease Aβ generation, resulting in early-onset AD or protection against developing AD. Mice completely deficient in BACE1 show nearly abolished Aβ production (Cai et al., 2001; Luo et al., 2001; Roberds et al., 2001), further confirming that BACE1 is an important target for AD treatment.

However, the use of BACE1 inhibition is not without concerns. Mice with BACE1 ablation exhibit abnormal astrogenesis, reduced neurogenesis, hyperactivities, impaired axonal growth and pathfinding, hypomyelination, altered long-term potentiation (LTP), and long-term depression, as well as defects in muscle spindles (see reviews in Vassar et al., 2014; Yan and Vassar, 2014; Barão et al., 2016; Hu et al., 2016). These phenotypes appear to be related to the abolished cleavage of BACE1 cellular substrates such as neuregulin-1 (Nrg1), Jagged 1 (Jag1), close homologue of L1, seizure protein 6, and voltage-gated sodium channel protein β subunits.

To better understand how BACE1 inhibition in adults will benefit AD patients, we generated homozygous BACE1 flox (fl) mice in which the *BACE1* gene can be temporally and tissue-specifically ablated by inducible *Cre/lox* technology. We bred BACE1 conditional KO mice (BACE1$^{fl/fl}$ mice) with ubiquitin-Cre^{ER} mice, which express Cre-ER driven by the ubiquitin C promoter in almost all tissues after treatment with tamoxifen (Ruzankina et al., 2007). We found significantly reduced BACE1 expression in adult BACE1$^{fl/fl/UbcCreER}$ mice even before tamoxifen treatment, and ~50% deletion of BACE1 occurred after postnatal day 60 (P60). Hence, the 5xFAD mouse model was chosen for this study because of the development of amyloid plaques after P60 in this model (Oakley et al., 2006). Strikingly, deletion of BACE1 in adult 5xFAD mice showed a remarkable reversal of amyloid deposition. To our knowledge, this is the first evidence that amyloid plaques can be completely reversed by gradual deletion of BACE1 beginning in early developmental stages. More importantly, the reversal of amyloid deposition in this AD mouse model significantly reduced neuronal loss, and cognitive functions were improved. Hence, this knowledge provides a strong foundation for the concept that BACE1

Correspondence to Riqiang Yan: Riyan@uchc.edu; Xiangyou Hu: hux@ccf.org

R. Yan's present address is Dept. of Neuroscience, University of Connecticut School of Medicine, Farmington, CT.

© 2018 Hu et al. This article is distributed under the terms of an Attribution–Noncommercial–Share Alike–No Mirror Sites license for the first six months after the publication date (see http://www.rupress.org/terms/). After six months it is available under a Creative Commons License (Attribution–Noncommercial–Share Alike 4.0 International license, as described at https://creativecommons.org/licenses/by-nc-sa/4.0/).

The Rockefeller University Press
J. Exp. Med. 2018 Vol. 215 No. 3 927–940
https://doi.org/10.1084/jem.20171831

inhibitors should be administered to humans as early as possible to prevent or reverse amyloid deposition. However, we also demonstrate that caution is warranted, as BACE1 itself is required for optimal cognitive functions.

RESULTS

BACE1 deletion in the adult mouse precludes early developmental defects

To generate BACE1 conditional KO mice, we designed a targeting vector with two loxP sites flanking exon 2 of the *BACE1* gene (Fig. S1, A–C). After F1 founder mice were identified, we crossed them with the flippase (FLP) deleter strain *Tg-ACTFLPe* to delete the *FRT*-flanked neomycin resistance (Neo) cassette and to obtain the final conditional BACE1$^{fl/fl}$ mice. BACE1$^{fl/fl}$ mice in C57BL/6J background were generated by crossing with C57BL/6J mice for over six generations and were maintained for subsequent functional and phenotypic analyses. By visual inspection, we noted that BACE1$^{fl/fl}$ mice grew normally and showed no visible differences compared with WT C57BL/6J mice. Western blot analyses confirmed no significant alterations in BACE1 expression when no Cre-recombinase gene was introduced (Fig. S1 D).

We then crossed BACE1$^{fl/fl}$ mice with UBC-Cre/*ER*^{T2} mice (007001; Jackson Laboratory), which presumably express Cre-ER driven by the ubiquitin C promoter in broad cell populations when treated with tamoxifen (Ruzankina et al., 2007). In our initial examination of BACE1$^{fl/fl/UbcCreER}$ mice, we surprisingly discovered that expression of BACE1 in protein lysates from 2- and 4-mo-old mice was significantly reduced in BACE1$^{fl/fl/UbcCreER}$ mice, even before tamoxifen treatment, suggesting a potential leakage of Cre expression in the UBC-Cre/*ER*$^{T2\ driver}$ mice. Because leaked expression of Cre in this driver line of mice has never been reported in the literature, we then bred UBC-Cre/*ER*^{T2} mice with a Cre reporter line R26R (Gt(ROSA)26Sor^{tm1Sor}/J) to monitor Cre-mediated (β-galactosidase) LacZ expression during development. We showed that LacZ was sparsely detected in the cortex and hippocampus beginning at the age of P45 in UbcCreER/R26R mice and reached broad neuronal expression at the age of P90 (Fig. 1 A). Further confocal staining confirmed that expression of β-galactosidase in UbcCreER/R26R mice was mainly in neurons and was not obviously observed in microglia or astrocytes (Fig. 1 B). β-Galactosidase was detected in neurons from broad brain regions, but only weakly in the lung (Fig. S2). This observation suggests that BACE1 deletion in BACE1$^{fl/fl/UbcCreER}$ mice can be attained in the adult even without tamoxifen treatment.

BACE1 expression and activity are well correlated with cleavage of its cellular substrates (Yan, 2017). We showed that BACE1 levels were not visibly different between P7 BACE1$^{fl/fl}$ and BACE1$^{fl/fl/UbcCreER}$ mice (Fig. 2 A), consistent with the aforementioned LacZ reporter expression. Levels of its substrates such as Jag1 were not significantly altered, and its downstream signaling molecules such as Notch intracellular domain and brain lipid–binding protein (BLBP) were also not visibly altered. BACE1 substrate type I Nrg1 was not detectable at this age. At the age of P20, BACE1 levels were also similar: Nrg1 was expressed, but levels of full-length Nrg1 were not significantly altered (see quantitative comparisons in Fig. 2 B). At this age, myelination was active, and myelin proteins such as myelin basic protein (MBP) and proteolipid protein (PLP) were strongly expressed, but no significant changes in either of these two proteins were detected.

With the growth of mice to P30 and P60, BACE1 levels were reduced in BACE1$^{fl/fl/UbcCreER}$ mice compared with BACE1$^{fl/fl}$ littermates, reaching ~50% at P60. However, at P120, BACE1 levels were reduced by ~80% (Fig. 2 C), reflecting a continuing expression of Cre at later ages. This significant reduction also caused a corresponding elevation in full-length Nrg1 as a result of decreased cleavage. Consequently, less Nrg1 bound to ErbB receptors to transmit signals, and thus, expression of downstream molecules such as MBP and PLP was decreased (Fig. 2, A and B). These results confirmed sequential and increased deletion of BACE1 in BACE1$^{fl/fl/UbcCreER}$ mice in an age-dependent manner.

Although cleavage of Nrg1 was reduced, and levels of MBP and PLP were decreased, we found no significant impact of reduced Nrg1 signaling on myelin sheath thickness in adult BACE1$^{fl/fl/UbcCreER}$ mice (an example of 5-mo-old nerves is shown in Fig. S3), likely as a result of passing a critical developmental stage for myelination. Unlike that seen in the BACE1-null dentate gyrus, we found no visible changes in astrogenesis in P30 and P60 BACE1$^{fl/fl/UbcCreER}$ mice (Fig. S4) when compared with BACE1$^{fl/fl}$ littermates, consistent with the important role of Jag-Notch signaling for the control of neurogenesis and astrogenesis in early developmental stages. Together, these data show that sequential deletion of BACE1 after early developmental stages avoids developmental defects that are normally observed in mice with germline deletion of BACE1.

Sequential deletion of BACE1 reverses neuritic plaques in a 5xFAD mouse model

Because BACE1 was largely deleted after P90, we then chose to cross BACE1$^{fl/fl/UbcCreER}$ mice with 5xFAD mice, which begin to develop amyloid plaques at the age of P75 as a result of the overexpression of familial APP and PS1 mutations (Oakley et al., 2006). Amyloid plaques initially develop in the subiculum and gradually spread to other hippocampal and broad cortical regions. We first obtained BACE1$^{fl/fl/5xFAD}$ mice to breed them with BACE1$^{fl/fl/UbeCrcER}$ mice. The obtained BACE1$^{fl/fl/UbcCreER/5xFAD}$ mice were compared with BACE1$^{fl/fl/5xFAD}$ mice for amyloid plaque development. We showed that both genotypes of mice (BACE1$^{fl/fl/5xFAD}$ and BACE1$^{fl/fl/UbcCreER/5xFAD}$) developed amyloid plaques at P75 at a comparable rate (Fig. 3 A), indicating no obvious effect of the small reduction in BACE1 on the formation of amyloid plaques. However, a clearer disparity developed with increasing age. BACE1$^{fl/fl/5xFAD}$ mice exhibited significantly increased plaque loads in an age-dependent manner and reached a high

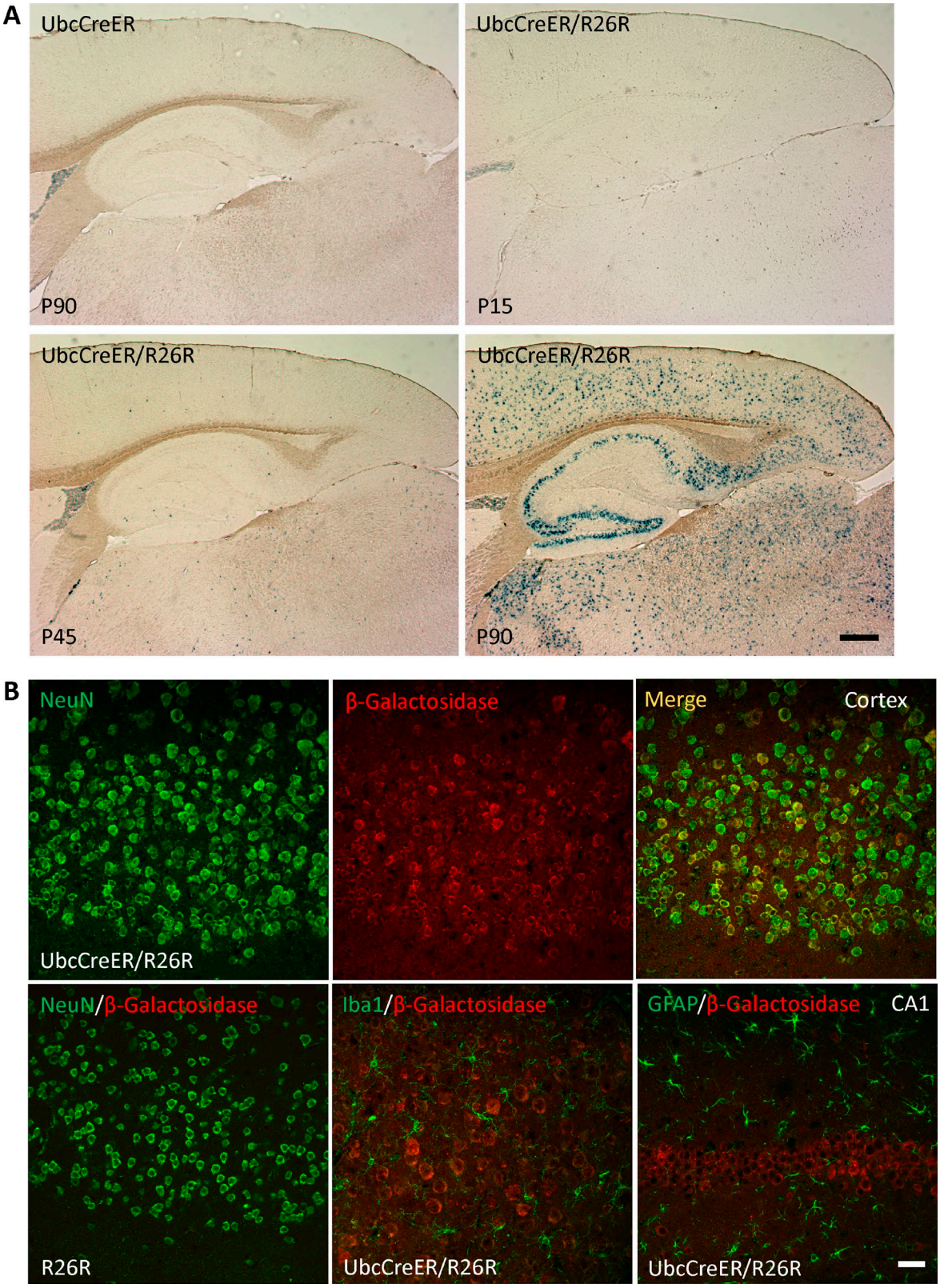
A
UbcCreER
P90
UbcCreER/R26R
P15
UbcCreER/R26R
P45
UbcCreER/R26R
P90
B
NeuN
UbcCreER/R26R
β-Galactosidase
Merge
Cortex
NeuN/β-Galactosidase
R26R
Iba1/β-Galactosidase
UbcCreER/R26R
GFAP/β-Galactosidase
CA1
UbcCreER/R26R

density of plaques in the frontal cortex and hippocampus at P300 (Fig. 3 A). Plaque loads in BACE1$^{fl/fl/UbcCreER/5xFAD}$ mice were greater at P120 than at P75, indicating a clear growth of plaque density during this period. Strikingly, the plaque load was decreased at P190 and was essentially undetectable at P300, suggesting a reversal of amyloid deposition when additional BACE1 was deleted. Further quantification confirmed that BACE1$^{fl/fl/5xFAD}$ mice had 31.7 ± 4.9 amyloid plaques in the cortex at P75, whereas BACE1$^{fl/fl/UbcCreER/5xFAD}$ mice had 24 ± 4.6 amyloid plaques in comparable regions (Fig. 3 B). With increasing age, BACE1$^{fl/fl/5xFAD}$ mice continuously accumulated more cortical amyloid plaques: 313.3 ± 48.2 at the age of P120, 444.9 ± 22.1 at the age of P190, and 778.5 ± 8.2 at the age of P300 (n = 6 mice in each age group). Comparably, BACE1$^{fl/fl/UbcCreER/5xFAD}$ mice at the age of P120 had 115.9 ± 10.7 amyloid plaques, which was 63% less than BACE1$^{fl/fl/5xFAD}$ mice but was still significantly higher than the numbers of amyloid plaques at the age of P75. However, with the continuing deletion of BACE1, amyloid plaque load at the age of P190 and P300 was reduced to 6.7 ± 4.6 in P190 BACE1$^{fl/fl/UbcCreER/5xFAD}$ mice and was barely visible in P300 BACE1$^{fl/fl/UbcCreER/5xFAD}$ mice (Fig. 3 B; n = 6 pairs; **, $P < 0.01$; ***, $P < 0.001$; Student's t test). Plaque reduction in the BACE1$^{fl/fl/UbcCreER/5xFAD}$ hippocampus was on a similar scale (Fig. 3 C).

We also conducted biochemical analyses of APP-processing products. The mean reduction of BACE1 reached ~40% at P30 (Fig. 4 A) and was >50% at P75 in BACE1$^{fl/fl/UbcCreER/5xFAD}$ mice (Fig. 4, A and quantification in B). We found that BACE1 conditional deletion at P75 had a relatively weak effect on APP-C99, which is a BACE1-cleaved APP C-terminal fragment detected by both antibodies A8717 (recognizing the APP C terminus) and 6E10 (recognizing the N-terminal end of Aβ; Fig. 4 A). The reduction of APP-C99 generation was highly correlated with BACE1 reduction, showing a more significant reduction after P120 compared with control littermates, and was essentially undetectable in P300 BACE1$^{fl/fl/UbcCreER/5xFAD}$ mice (Fig., 4 A and B). Intriguingly, an increase in APP-C83, which is the product of APP cleavage by α-secretase, appeared to be inversely correlated with the reduction of C99 at early time points (P75) but was significantly reduced concomitantly with the loss of C99 in older BACE1$^{fl/fl/UbcCreER/5xFAD}$ mice, especially at P300 (Fig. 4 A).

Quantification of Aβ by ELISA showed consistent results: an age-dependent sequential increase in $A\beta_{40}$ (Fig. 4 C) and $A\beta_{42}$ (Fig. 4 D) in BACE1$^{fl/fl/5xFAD}$ mice and a sequential reduction in both $A\beta_{40}$ and $A\beta_{42}$ in older BACE1$^{fl/fl/UbcCreER/5xFAD}$ mice. At the age of P300, the reductions in $A\beta_{40}$ and $A\beta_{42}$ were by ~97% and ~97.5%, respectively, consistent with the essentially abolished amyloid plaques in P300 BACE1$^{fl/fl/UbcCreER/5xFAD}$ mice. Collectively, these results demonstrate that significant and sequential inhibition of BACE1 in an age-dependent manner completely reverses amyloid deposition in the late adult stage. To our knowledge, this is the first observation of such a dramatic reversal of amyloid deposition in any study of AD mouse models.

Decreased amyloid deposition reverses gliosis and dystrophic neurites in a 5xFAD mouse model

To determine whether sequential deletion of BACE1 affects gliosis, we examined fixed brain sections with Iba1 antibody to label microglia. We showed that activated microglia, as labeled by Iba1, were correlated with amyloid plaque density (Fig. S5, A–C) and that activated microglia were clearly associated with amyloid plaques (Fig. 5 A). In BACE1$^{fl/fl/UbcCreER/5xFAD}$ mice, levels of activated microglia with clear ramified and amoeboid morphology were smaller at P75 but were significantly greater at P120 and returned to barely detectable levels at P300 (Fig. 5 A and Fig. S5 C), suggesting that their activation is reversible and is correlated with amyloid deposition. In parallel, the density of reactive astrocytes, as labeled by Smi22 for glial fibrillary acidic protein (GFAP), was also correlated with amyloid plaque loads: It was low at P75, higher at P120, and returned to resting levels at P300 BACE1$^{fl/fl/UbcCreER/5xFAD}$ (Fig. 5 B).

We also examined dystrophic neurites labeled by reticulon-3 (RTN3) or ubiquitin antibody. RTN3-immunoreactive dystrophic neurites (RIDNs) were readily observed surrounding amyloid plaques beginning in P75 BACE1$^{fl/fl/5xFAD}$ mice (Fig. 5 C). Ubiquitin-labeled dystrophic neurites were not yet detectable at this age but were visible at older ages (Fig. S5 D). Noticeably, dispersed RIDNs were not evident at P75 but were readily observed in both BACE1$^{fl/fl/5xFAD}$ and BACE1$^{fl/fl/UbcCreER/5xFAD}$ mice at P120 (Fig. 5 C, arrows). Ubiquitin-labeled dystrophic neurites mostly surrounded amyloid plaques and were not in dispersed form, indicating the presence of two populations of dystrophic neurites and that RIDNs likely result from enrichment in RTN3-containing tubular ER (Sharoar et al., 2016). At P300, RIDNs (Fig. 5 C) and ubiquitin-labeled dystrophic neurites (Fig. S5 D) were essentially absent from BACE1$^{fl/fl/UbcCreER/5xFAD}$ mouse brains, in line with the abolished amyloid deposition. This is in contrast to P300 BACE1$^{fl/fl/5xFAD}$ mouse brains, in which neuritic dystrophy was more dramatic and exhibited a higher density of dispersed RIDNs (Fig. 5 C). Noticeably, dispersed RIDNs

Figure 1. **Characterization of Cre recombinase expression in UBC-Cre/*ER^{T2}* mice. (A)** Gt(ROSA)26Sor^{tm1Sor}/J Cre-reporter mice were bred with UBC-Cre/*ER^{T2}* mice to monitor expression of Cre recombinase in the brain, as detected by expression of β-galactosidase. Expression of LacZ, as detected by X-Gal, in P15 brains was sporadic and not readily detected. LacZ was detectable at P45 and was more prominent at P90 in compound mice. Bar, 200 µm. **(B)** Confocal staining was conducted to monitor the expression of β-galactosidase in neurons (labeled by NeuN antibody), microglia (Iba1 antibody), or astrocytes (Smi22 for GFAP) in P90 compound mice or control littermates. Bar, 100 µm.

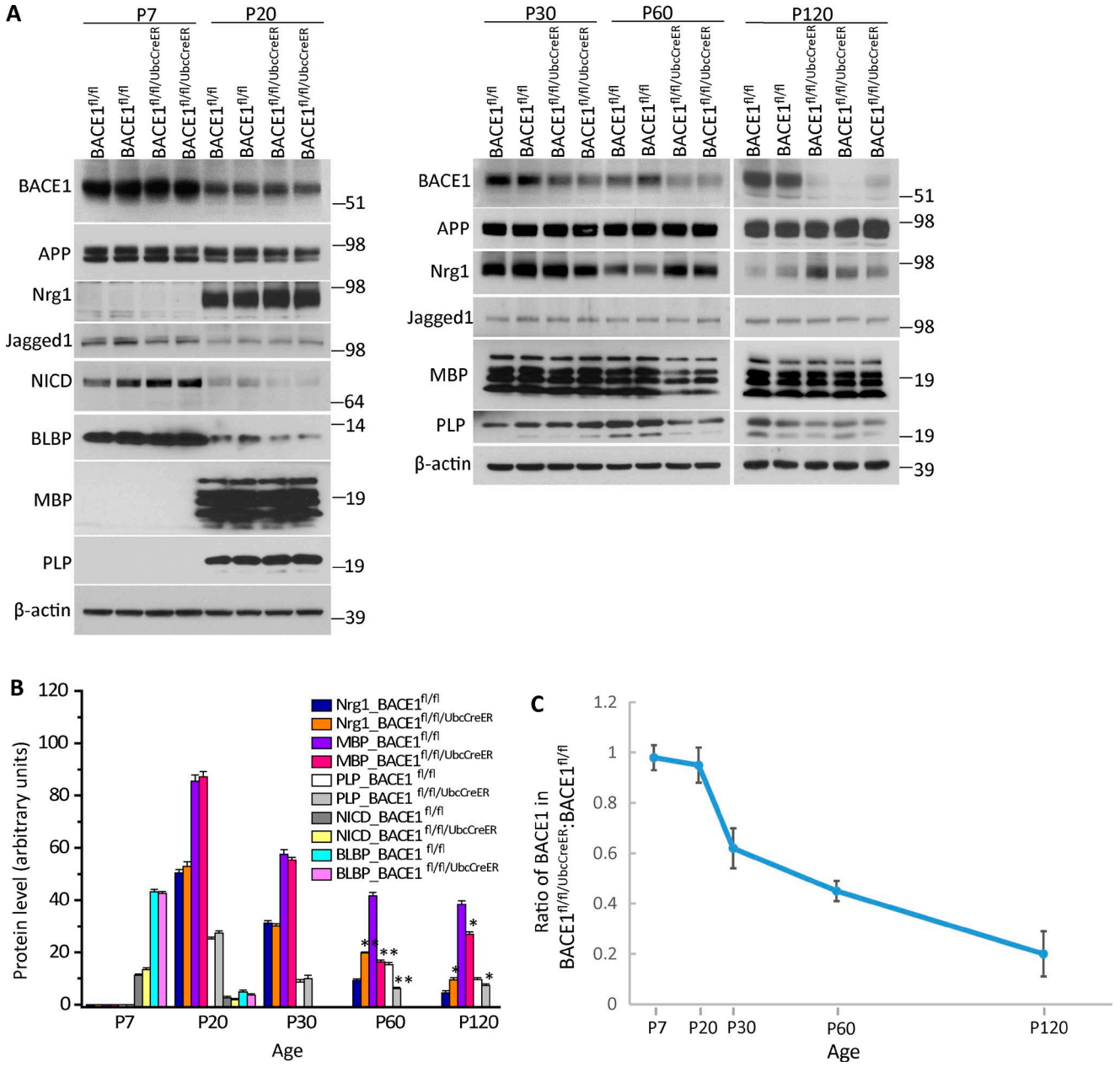

Figure 2. **Sequential deletion of BACE1 in adult mice. (A)** BACE1$^{fl/fl}$ mice were crossed with UBC-Cre/*ER*^{T2} mice to obtain BACE1$^{fl/fl/UbcCreER}$ mice, and expression of BACE1 in BACE1$^{fl/fl/UbcCreER}$ mice was examined at different ages (P7–P120). BACE1 substrates such as APP, Nrg1, and Jag1, as well as selected relevant downstream molecules such as Notch intracellular domain (NICD), MBP, PLP, and BLBP, were also examined in parallel. Molecular mass is indicated in kilodaltons. Antibody to β-actin was used to verify equal loading. **(B)** Bar graphs show the arbitrary levels of specified proteins in different age groups (n = 3 independent experiments; two or three animals in each age group were compared side by side; *, $P < 0.05$, **, $P < 0.01$; two-tailed Student's t test). **(C)** Ratios of BACE1 levels in BACE1$^{fl/fl/UbcCreER}$ mice to BACE1$^{fl/fl}$ mice in different age groups are plotted (n = 6–9 animals in each group). BACE1 levels were reduced by ~80% in P120 BACE1$^{fl/fl/UbcCreER}$ mice. Values are expressed as mean ± SEM.

sporadically remained in P300 BACE1$^{fl/fl/UbcCreER/5xFAD}$ mouse hippocampi. Together, these results show that a significant reduction in BACE1 activity in older 5xFAD mice not only reverses gliosis, but also significantly reduces neuritic dystrophy.

Decreased amyloid deposition partially reverses cognitive dysfunction in a 5xFAD mouse model

Abnormal accumulation of Aβ in the form of dimers, trimers, or oligomers is highly correlated with synaptic dysfunc-

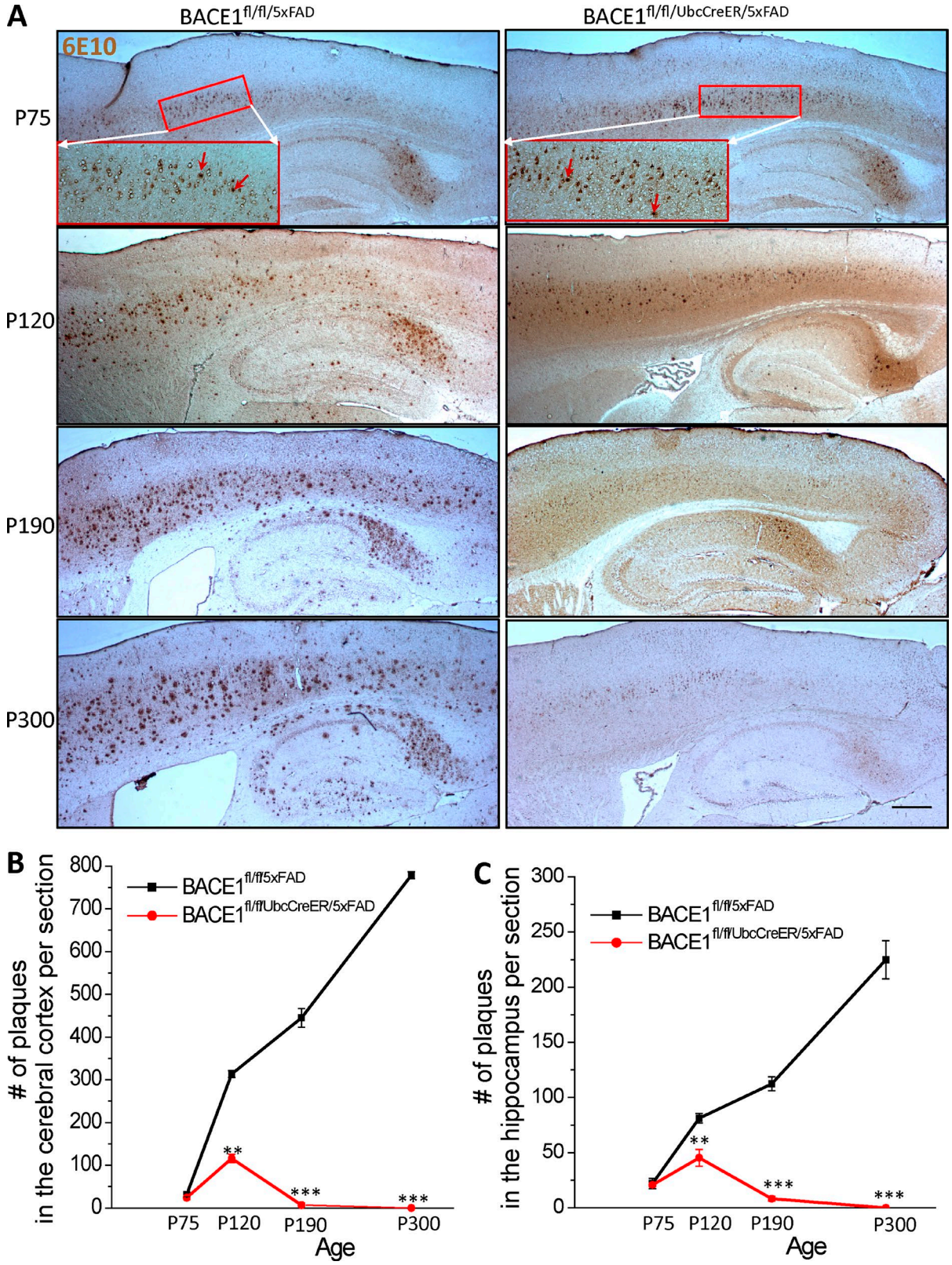

Figure 3. **Reversal of amyloid deposition in an adult AD mouse model produced by sequentially increasing deletion of BACE1. (A)** Fixed brain sections from different age groups of the indicated genotypes of mice were stained with antibody 6E10 to label amyloid plaques. A sequential increase in amyloid plaque load in BACE1$^{fl/fl/5xFAD}$ mice from P75, P120, P190, and P300 was visible. Enlarged views show differences in neurons and amyloid plaques,

tions, including impairments in LTP and cognitive functions (Malenka and Malinow, 2011). We recorded LTP on hippocampal slices prepared from four different genotypes of mice: BACE1$^{fl/fl/5XFAD}$, BACE1$^{fl/fl/UbcCreER}$, BACE1$^{fl/fl/UbcCreER/5XFAD}$, and BACE1$^{fl/fl}$. LTP was induced in Schaffer collateral–CA1 synapses by applying theta burst stimulations (TBSs), and the amplitudes of field excitatory postsynaptic potentials (fEPSPs) were compared. BACE1$^{fl/fl}$ mice elicited a typical LTP lasting >40 min with 160.2 ± 8% of the mean fEPSP amplitude at 30 min after TBS (Fig. 6 A, blue line; 10 mo of age, n = 8 slices). However, 5xFAD mice (BACE1$^{fl/fl/5xFAD}$ mice) exhibited significantly impaired LTP, with a mean fEPSP amplitude of only 104.6 ± 2% at 30 min after TBS (Fig. 6 A, red line; n = 8 slices; **, P < 0.01; Student's t test), and this impairment was age dependent because younger BACE1$^{fl/fl/5xFAD}$ mice exhibited stronger LTP (Fig. 6 B, pink line; 4–5 vs. 10 mo, n = 8 slices). When amyloid plaques were removed in BACE1$^{fl/fl/UbcCreER/5xFAD}$ mice, LTP in these mice was partially restored, with the mean fEPSP amplitude reaching 121.3 ± 4% (Fig. 6 C, black line; n = 8 slices; *, P < 0.05 when compared with BACE1$^{fl/fl/5XFAD}$ mice; Student's t test). This partial improvement was related to the deletion of BACE1 in the adult, as we found no differences in mean fEPSP amplitude between BACE1$^{fl/fl/UbcCreER/5xFAD}$ mice and BACE1$^{fl/fl/ubcCreER}$ mice, which was 127.5 ± 6% in fEPSP amplitude (Fig. 6 D; n = 8 slices; P > 0.05, Student's t test). The overlay of these traces showed clear partial impairment of LTP upon deletion of BACE1 in the adult (Fig. 6, E and F) when comparing the five different conditions.

Improved learning and behavior in a 5xFAD mouse model with BACE1 reduction

Although BACE1 deletion in the adult decreases LTP, we actually found improved learning and memory as measured by a contextual fear conditioning test, which is one of the most commonly used paradigms to assess cognitive function in rodents (Bach et al., 1995). In this experiment, four genotypes of 8–10-mo-old mice were subjected to the standard 3-d test. In the preconditioning test on day 1, mice were placed in the fear conditioning chamber and exposed to a sound followed by a foot shock. There were no significant differences among the different genotypes of mice in the percentage of freezing time (Fig. 7). Context-dependent freezing was recorded on day 2 by placing mice back in the same chamber, but without exposure to the sound or shock. We found that freezing time was lowered in 5xFAD mice (Fig. 7; 35.47 ± 4.75% in 20 BACE1$^{fl/fl/5xFAD}$ mice vs. 41.62 ± 4.51% in 15 BACE1$^{fl/fl}$ mice, P = 0.23), consistent with the reduction in LTP exhibited in BACE1$^{fl/fl/5xFAD}$ mice. Freezing time in BACE1$^{fl/fl/UbcCreER}$ mice was 42.16 ± 7.62% (n = 14), which was comparable with BACE1$^{fl/fl}$ mice and suggested no obvious impairment in learning and memory when BACE1 was deleted. Remarkably, a reversal in freezing time was seen in BACE1$^{fl/fl/UbcCreER/5xFAD}$ mice (49.77 ± 4.32%; n = 25; *, P < 0.05; Student's t test), indicating that removal of amyloid plaques improves performance on the contextual fear conditioning test. On day 3 for the cue test, the freezing time in BACE1$^{fl/fl/5xFAD}$ mice was also reduced but did not reach statistical significance when compared with the other three genotypes of mice (Fig. 7). Thus, our behavioral tests indicate an improved learning and memory after BACE1 deletion in adult 5xFAD mice.

DISCUSSION

AD is widely regarded as a disease of synaptic failure associated with age-dependent neurodegeneration. Abnormal accumulation of Aβ is an early event that leads to the eventual formation of amyloid plaques, neurofibrillary tangles, and cognitive dysfunction (Selkoe and Hardy, 2016). BACE1 is a critical enzyme for Aβ generation, and BACE1 inhibitors are being actively developed to treat AD patients (Vassar, 2014; Yan, 2016). Ideally, BACE1 inhibitors should have manageable side effects, as BACE1 inhibitors are expected for long-term use. We developed conditional BACE1 KO mice for the purpose of deleting BACE1 at the adult stage to mimic inhibition of BACE1 in AD patients. Using this model, we investigated how BACE1 deletion in adults impacts the development of amyloid deposition and related pathological changes. In this study, we provide genetic evidence that sequential and gradually increased deletion of BACE1 not only reverses existing amyloid plaques, but also reduces gliosis and neuritic dystrophy and improves synaptic functions.

We showed that inhibition of BACE1 has multiple beneficial effects. Not only can it reduce Aβ generation and amyloid deposition, but it can also reduce levels of other potentially toxic APP-processing products such as APP intracellular domain (AICD). BACE1-cleaved C-terminal fragment (APP-C99) was previously shown to impair synaptic functions (Tamayev et al., 2012), endosomal function (Kim et al., 2016), and lysosomal-autophagic function (Lauritzen et al., 2016). BACE1 inhibition clearly reduces APP-C99 production in early stages, and its production is nearly abolished at later stages (Fig. 4). In P300 BACE1$^{fl/fl/UbcCreER/5xFAD}$ mice, dystrophic neurites were significantly reduced (Fig. 5 C), in line with the reduction of both Aβ and APP-C99. Noticeably, in P300 BACE1$^{fl/fl/UbcCreER/5xFAD}$ mice, we also observed a clear reduction in APP-C83, which is produced by α-secretase cleavage of APP. BACE1 and α-secretase are expected to compete to cleave APP to produce APP-C99 and

which are indicated by red arrows. No amyloid plaques were observed in P300 BACE1$^{fl/fl/UbcCreER/5xFAD}$ mice, whereas a high load of amyloid plaques was observed in P120 BACE1$^{fl/fl/UbcCreER/5xFAD}$ mice. Bar, 200 µm. **(B and C)** Numbers of 6E10-positive plaques in the cortex (B) and hippocampus (C) were quantified from six animals in each age group, and mean numbers per section are plotted for comparison (**, P < 0.01; ***, P < 0.001; two-tailed Student's t test). Plaque load was significantly reduced in BACE1$^{fl/fl/UbcCreER/5xFAD}$ mice older than P120 compared with BACE1$^{fl/fl/5xFAD}$ littermates. Values are expressed as mean ± SEM.

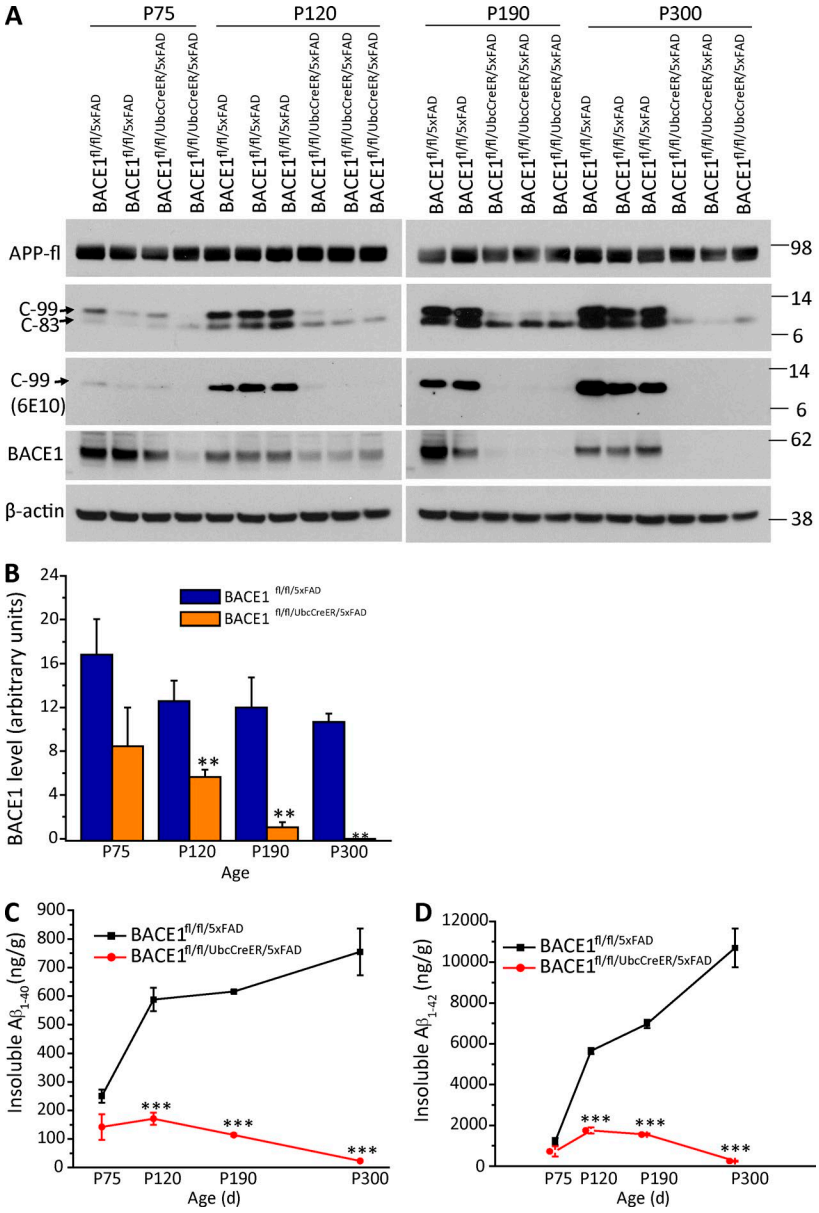

Figure 4. **Sequentially increased deletion of BACE1 reduces APP processing and Aβ generation. (A)** APP processing products were examined by Western blot analyses. C99 is a BACE1-cleaved APP C-terminal fragment, which was detected by both antibody 6E10 and A8717, which recognize the APP C terminus. Antibody A8717 also detects C83, which is a product resulting from α-secretase cleavage of APP. Antibody to β-actin was used to verify equal loading. Blot measurements in kilodaltons. **(B)** Relative levels of BACE1 in different age groups are plotted for comparison (equal to at least six animals in each genotype and age group). Significantly less C83 and C99 were observed in BACE1$^{fl/fl/UbcCreER/5xFAD}$ mice compared with BACE1$^{fl/fl/5xFAD}$ mice beginning at P120. **(C and D)** Insoluble $A\beta_{40}$ and $A\beta_{42}$ from mouse hippocampal regions were extracted and measured by standard ELISA methods (n = 6 pairs of animals; **, $P < 0.01$; ***, $P < 0.001$; two-tailed Student's t test). Values are expressed as mean ± SEM.

-C83. Reduction in both products was unexpected, and the reason for this is not yet clear. One potential explanation is that it is caused by enhanced degradation of these fragments by improved lysosomal-autophagic function. An improved lysosomal-autophagic function is likely to be beneficial for AD patients and should be investigated in more detail in the future.

Nevertheless, significant inhibition of BACE1 in the adult is not without concern. In BACE1$^{fl/fl/UbcCreER/5xFAD}$ mice, we noted an age-dependent reduction in LTP (Fig. 6 B) and that impaired LTP reverted to a level similar to BACE1$^{fl/fl/UbcCreER}$ mice, but not control levels in BACE1$^{fl/fl}$ mice (Fig. 6 E), indicating that BACE1 in the adult is required for optimal LTP. Our results also suggest that significant inhibition of BACE1 in the adult is likely to have side effects associated with the full recovery of cognitive function in AD patients. As demonstrated in our study (Fig. 2, B and C), partial deletion of BACE1 impacts cleavage of Nrg1, and this is likely related to the high affinity between BACE1 and Nrg1 (Ben Halima et al., 2016). BACE1 cleavage of Nrg1 releases its epidermal growth factor domain–containing N-terminal fragment, which binds to ErbB receptors in inhibitory neurons to control synaptic functions (Mei and Nave, 2014), and the deletion of BACE1 reduces this signaling capacity and likely alters synaptic transmission. Further studies will be needed to elucidate whether Nrg1 or other BACE1 substrates are responsible for the partial reduction in LTP. Despite this, we found that BACE1$^{fl/fl/UbcCreER/5xFAD}$ mice appeared to behave normally in the contextual fear conditioning test. This difference between electrophysiological recording results and learning and memory behaviors is likely a result of multiple factors, which include the relatively young age of

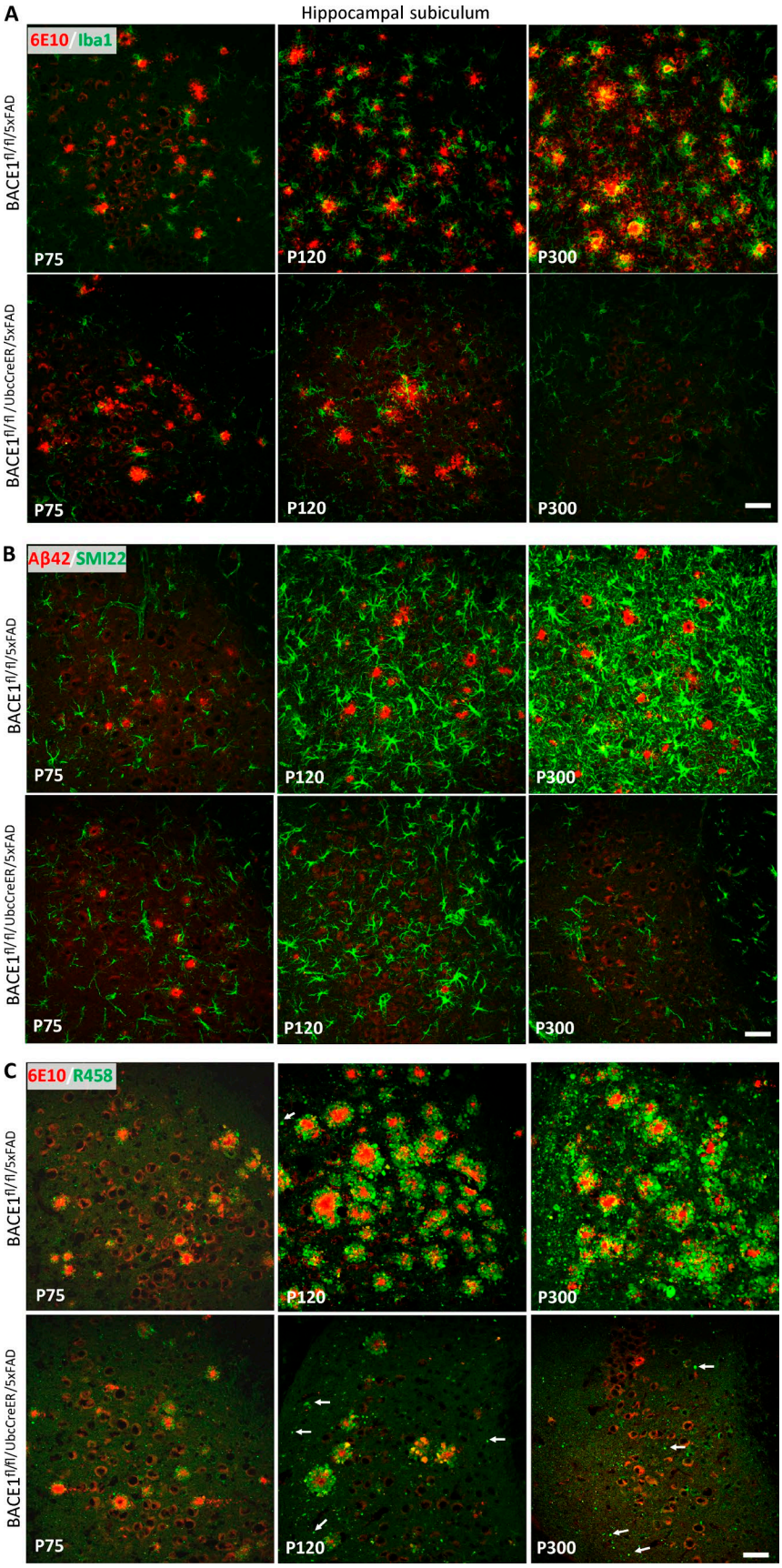

Figure 5. **Reversal of gliosis and neuritic dystrophy is associated with removal of amyloid plaques. (A)** Fixed brain sections from P75, P120, and P300 mice were stained with antibody 6E10 to label amyloid plaques and Iba1 to label microglia. **(B)** Similar brain sections were stained with an IBL antibody specific to $A\beta_{42}$ to label core amyloid plaques. Astrocytes were labeled by Smi22 antibody, which is specific to GFAP. **(C)** Although amyloid plaques were labeled by antibody 6E10, dystrophic neurites were labeled by antibody R458, which is specific to the C terminus of RTN3. Dystrophic neurites were formed in correlation with amyloid plaque density in older 5xFAD mice but were essentially absent when plaques were cleared in P300 $BACE1^{fl/fl/UbcCreER/5xFAD}$ mice. All images were captured from hippocampal subiculum. Bars, 40 µm. White arrows indicate the dispersed dystrophic neurites, which were labeled by R458 antibody.

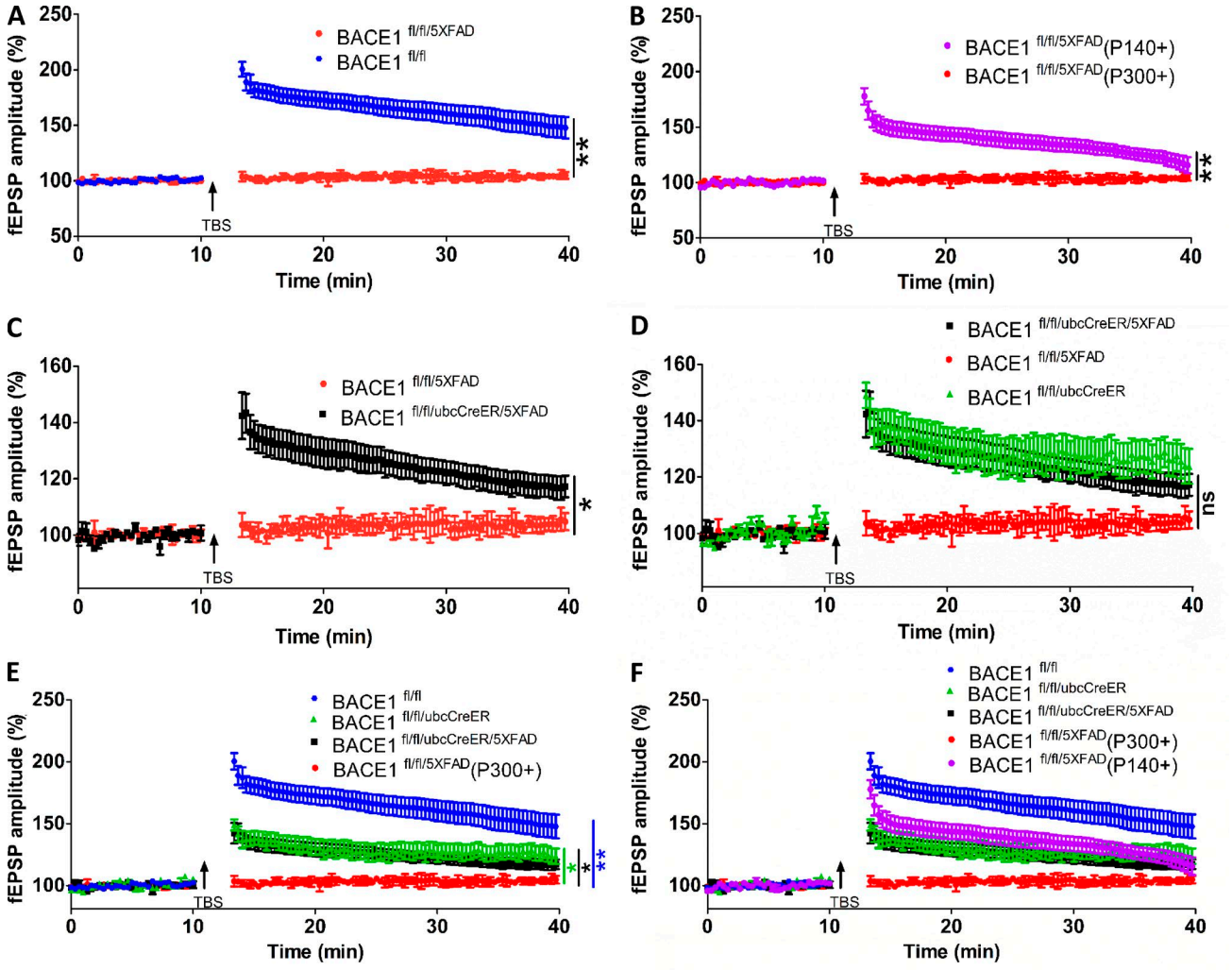

Figure 6. **BACE1 deletion in the adult impacts LTP. (A–D)** LTP was recorded on horizontal hippocampal slices from four genotypes of 10–12-mo-old mice using the MED64 system, and Schaffer collaterals to CA1 synapses were analyzed for LTP assays. Comparison between BACE1$^{fl/fl}$ mice and BACE1$^{fl/fl/5xFAD}$ littermates is shown in A. (B) LTP was also recorded on horizontal hippocampal slices from 4–5-mo-old (labeled as P140+) BACE1$^{fl/fl/5xFAD}$ mice and compared with that from 10–12-mo-old (P300+) BACE1$^{fl/fl/5xFAD}$ mice (n = 8–10 slices). Comparison between BACE1$^{fl/fl/5xFAD}$ mice and BACE1$^{fl/fl/UbcCreER/5xFAD}$ mice is shown in C (Student's t test). There was no significant difference in LTP between BACE1$^{fl/fl/UbcCreER}$ mice and BACE1$^{fl/fl/UbcCreER/5xFAD}$ mice (D). **(E and F)** Comparisons of all four genotypes of mice are shown in E, and all five groups are shown in F. *, $P < 0.05$; **, $P < 0.01$; Student's t test. ns, no significance. Values are expressed as mean ± SEM.

behaviorally tested animals and potential compensatory effects in BACE1$^{fl/fl/UbcCreER/5xFAD}$ mice, as well as weak behavioral impairments exhibited in BACE1$^{fl/fl/5xFAD}$ mice.

To our knowledge, this study provides the first evidence that preformed amyloid deposition can be completely reversed after sequential and increased deletion of BACE1 in adults. Partial inhibition of BACE1, i.e., by 50% in heterozygous BACE1 KO mice, is not sufficient to dramatically reduce amyloid plaques in all age groups (Sadleir et al., 2015). Although it is expected that BACE1 inhibition in our model will gradually decrease the production of Aβ, it is intriguing that amyloid plaques are actually cleared and removed in old BACE1$^{fl/fl/UbcCreER/5xFAD}$ mice. Potential factors in this clearance are the effects produced by microglia. 6–10-mo-old BACE1$^{fl/fl/UbcCreER/5xFAD}$ mice are still considered to be relatively young, and microglia are fully functional in removing amyloid plaques, as demonstrated in a recent study (Daria et al., 2017). It will be interesting to test whether significant deletion of BACE1 in older AD mice will also result in clearance of preformed amyloid plaques by microglia or whether additional components to enhance microglial function are required for full clearance of amyloid plaques. Enhanced lysosomal-autophagic functions are postulated to contribute to the degradation of aggregated Aβ.

In summary, our data in this study show that BACE1 inhibition has the full potential to treat AD patients if the

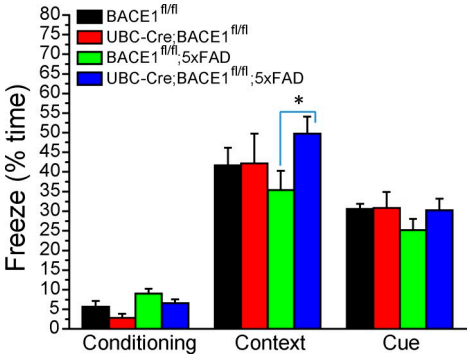

Figure 7. **BACE1 deletion in the adult 5xFAD mouse model ameliorates learning and behavioral impairments.** A fear conditioning assay was conducted for 3 d using standard procedures. There were no differences in the percentage of freeze time during the day 1 preconditioning test. On day 2, contextual fear learning and memory of the mice were analyzed. Changes in total freeze time on day 2 are reflected in their contextual learning ability. BACE1$^{fl/fl/5xFAD}$ mice (n = 20) showed significantly less freezing time compared with BACE1$^{fl/fl/UbcCreER/5xFAD}$ mice (n = 25; *, $P < 0.05$). Day 3 measured tone-mediated cue memory by comparing freezing during the presentation of tones in a different chamber, which is more related to amygdala function, and no significant differences were noted among the four genotypes of mice. Values are expressed as mean ± SEM.

drug effectively crosses the blood–brain barrier and retains high potency to inhibit BACE1 activity. More importantly, BACE1 inhibitors should be devoid of unwanted and off-target chemical toxicity, and such drugs can be used in humans for long-term use. Our data also suggest that sequential and gradual increases in BACE1 inhibition are likely to be the most beneficial for AD patients. Future studies should further develop a strategy to minimize the synaptic impairments arising from significant inhibition of BACE1 to achieve maximal and optimal benefits for AD patients.

MATERIALS AND METHODS

Generation of BACE1 conditional KO mice

The *BACE1* gene contains nine exons spanning ~24 kb on the chromosome 9 forward strand. For conditional deletion of BACE1, we generated a conditional BACE1 KO mouse (*BACE1*$^{fl/fl}$ mouse) by using the targeting vector having two *loxP* sites flanking exon 2 of *BACE1*. Exon 2 is a common exon for all BACE1 isoforms, and the region around exon 2 does not include known regulatory elements. The targeting vector was confirmed by DNA sequencing, linearized by AscI digestion, and electroporated into C2 C57BL/6 embryonic stem (ES) cells, in which its 5′ arm (9.5 kb) and 3′ arm (8.3 kb) of homology underwent homologous recombination with the WT allele. Selection for homologous recombination was achieved by G418, which identifies ES cell clones that contain the Neo cassette present in the targeted allele. The Neo cassette is flanked with FLP recombinase target (*FRT*) sites to facilitate subsequent removal of the Neo cassette from founder mice (Fig. S1 A). Southern blotting using two different probes (see diagram of WT allele in Fig. S1 A) was performed to identify correctly targeted ES cell clones. A total of seven clones, confirmed by PCR genotyping with primers (forward: 5′-TCTGACGATGGCACACATAAGC-3′; reverse: 5′-TGCTAGTGTTTCCTGTCACCTG-3′) flanking the 5′ *loxp* sequence (Fig. S1 B), were determined to contain the targeted allele and validated by Southern blot analyses (probes illustrated in Fig. S1 C). The verified ES cell clones were microinjected into C57BL/6 blastocysts, and a total of 10 chimeras were further bred for germline transmission of the targeted allele in the F1 generation, which was confirmed by both PCR and Southern blotting. F1 founders were further crossed with the FLP deleter strain *Tg-ACTFLPe* (003800; Jackson Laboratory) to delete the *FRT*-flanked Neo cassette to generate the final conditional BACE1 KO mice (BACE1$^{fl/fl}$ mice). For maintenance, mice heterozygous for BACE1-floxed allele (BACE1$^{fl/+}$) in C57BL/6J background were genotyped by PCR with primers (forward: 5′-TCT GACGATGGCACACATAAGC-3′; reverse: 5′-TGCTAG TGTTTCCTGTCACCTG-3′). When needed, Southern blotting experiments were performed for further confirmation, and an example is shown in Fig. S1 C. All experimental protocols were approved by the Institutional Animal Care and Use Committee of the Lerner Research Institute in compliance with the guidelines established by the Public Health Service Guide for the Care and Use of Laboratory Animals.

Mouse strains and breeding strategy

BACE1$^{fl/+}$ mice were crossbred to generate mice homozygous for the floxed BACE1 allele (BACE1$^{fl/fl}$). BACE1$^{fl/fl}$ mice were bred with Tg (UBC-Cre/ER^{T2}) mice (007001; Jackson Laboratory) to obtain mice heterozygous for the transgenic Cre and homozygous for the floxed BACE1 (BACE1$^{fl/fl/UbcCreER}$) mice. BACE1$^{fl/fl}$ mice were bred with Tg (APPSwFlLon,PSEN1*M146L*L286V) mice (5xFAD; Jackson Laboratory) to obtain mice heterozygous for the transgenic 5xFAD and homozygous for floxed BACE1 (BACE1$^{fl/fl/5xFAD}$) mice. BACE1$^{fl/fl/5xFAD}$ male and BACE1$^{fl/fl/UbcCreER}$ females were mated to generate BACE1$^{fl/fl/UbcCreER/5xFAD}$, BACE1$^{fl/fl/5xFAD}$, BACE1$^{fl/fl/UbcCreER}$, and BACE1$^{fl/fl}$ offspring for this study. R26R (Gt(ROSA)26Sortm1Sor/J (003474) was purchased from the Jackson Laboratory. All lines were routinely backcrossed with C57BL/6J mice for at least five generations to ensure consistent genetic background for phenotypic analyses.

Immunofluorescent confocal microscopy

Confocal experiments were performed according to standard methods as previously described (He et al., 2004). The mouse brain was surgically removed, fixed in 4% paraformaldehyde for 12 h, and immersed in 20% sucrose overnight at 4°C. Brains were sagittally sectioned (16-µm thick) on a freezing microtome (Microm GmbH). Sections were permeabilized with 0.3% Triton X-100 for 30 min. After being rinsed in PBS three times to remove detergent, the sections were heated by

microwave in 0.05 M citrate-buffered saline, pH 6.0, for 5 min, blocked with 5% normal goat serum, and incubated with individual primary antibodies at the following dilutions: 6E10 (1:1,000; AB_662804; Signet), Iba1 (1:500; AB_839504; Wako Chemicals), SMI22 (1:1,000; AB_2313859; Covance), $A\beta_{1-42}$ (1:500; AB_2341375; IBL-American), Ubiquitin (1:1,000; AB_477667; Sigma), and R458 (1:1,000; Millipore; He et al., 2004). The quality of the R458 antibody was confirmed by Western blotting and immunohistochemical staining by utilizing RTN3 KO mice (Shi et al., 2014). After washing with PBS three times, sections were incubated with secondary antibodies conjugated with Alexa Fluor 488 or Alexa Fluor 568 (Molecular Probes).

Western blotting and antibodies

Protein extraction was performed according to previously described procedures (Hu et al., 2007). Brain samples were homogenized in radioimmunoprecipitation assay (RIPA) buffer (50 mM Tris–HCl, pH 7.4, 1% NP-40, 0.25% sodium deoxycholate, 150 mM NaCl, 1 mM EDTA, 1 mM NaF, 1 mM Na_3VO_4, and a protease inhibitor cocktail [Roche]) and centrifuged at 13,200 rpm for 90 min. Equal amounts of protein were resolved on a NuPAGE Bis-Tris gel (Invitrogen) and transferred onto nitrocellulose membranes (Invitrogen). Subsequently, blots were incubated with primary antibodies (1:1,000 APP-C [AB_258409; Sigma]; 1:1,000 BACE1; 1:200 type I Nrg1 [AB_2154793; Santa Cruz]; 1:200 Jag1 [AB_649685; Santa Cruz]; 1:1,000 BLBP [AB_10000325; Millipore]; 1:1,000 Cleaved Notch1 [AB_2153351; Cell Signaling]; 1:10,000 MBP [AB_510039; Sternberger Monoclonals]; 1:2,000 PLP; 1:2,000 6E10 [AB_662804; Signet]; 1:50,000 actin [AB_476744; Sigma]) overnight at 4°C. After extensive washing, blots were reacted with HRP-conjugated secondary antibodies and visualized using enhanced chemiluminescence (Thermo Scientific).

Quantification of Aβ peptides using ELISA

Insoluble $A\beta_{1-40}$ and $A\beta_{1-42}$ were differentially prepared from the frozen hippocampus by the guanidine hydrochloride method (Shi et al., 2014). Levels of $A\beta_{1-40}$ and $A\beta_{1-42}$ in hippocampal samples were quantified by sandwich ELISA according to previously described procedures (He et al., 2004). Results were obtained from six female $BACE1^{fl/fl/5xFAD}$ and six female $BACE1^{fl/fl/UbcCreER/5xFAD}$ hippocampal samples in each age group.

Quantification of amyloid plaque load

Quantification of amyloid plaques was conducted with serial sagittal sections, which were selected at 10-section intervals. Amyloid plaques were labeled with 6E10 antibody followed by 3,3′-diaminobenzidine visualization. Images were captured by a DMR microscope (Leica) with a charge-coupled device camera (Retiga-2000R; QImaging) using a 2.5× objective. Plaque numbers in the cerebral cortex and hippocampus were counted using ImageJ software (National Institutes of Health). Six female $BACE1^{fl/fl/5xFAD}$ and six female $BACE1^{fl/fl/UbcCreER/5xFAD}$ mice in each age group were used.

LTP recordings

LTP recordings on hippocampal slices were performed according to previously described procedures (Shimono et al., 2002; Baba et al., 2003; Itoh et al., 2005). In brief, horizontal hippocampal slices (350-µm thickness) were prepared from the brains of 10–12-mo-old $BACE1^{fl/fl/UbcCreER/5xFAD}$, $BACE1^{fl/fl/5xFAD}$, $BACE1^{fl/fl/UbcCreER}$, and $BACE1^{fl/fl}$ mice in ice-cold, 95% O_2/5% CO_2 oxygenated artificial cerebrospinal fluid consisting of the following ingredients: 124 mM NaCl, 3 mM KCl, 1.24 mM KH_2PO_4, 1.5 mM $MgSO_4$, 2.0 mM $CaCl_2$, 26 mM $NaHCO_3$, and 10 mM glucose. The prepared slices were incubated at room temperature for >1 h before recording. Slices were then placed onto the center of a MED probe (MED-P515A; AutoMate Scientific) and perfused in 95% O_2/5% CO_2–saturated artificial cerebrospinal fluid. The device had an array arranged in an 8 × 8 pattern of 64 planar microelectrodes across a hippocampal slice. Each electrode was 20 × 20 µm with an interelectrode distance of 150 µm. A SU-MED640 amplifier run by Mobius software was used for data acquisition and analysis. Schaffer collaterals to CA1 synapses were typically analyzed for LTP assays. fEPSPs caused by stimulation were recorded at a 20-kHz sampling rate. Control fEPSPs were recorded for at least 10 min before the conditioning stimulation. After a stable baseline was established, LTP was induced by TBS, which was a 10-burst train of four 100-Hz pulses with 200-ms intertrain intervals. Field potential amplitudes were then measured. Data are expressed as mean ± SEM. Synaptic strength was evaluated by measuring changes in the fEPSP amplitude relative to baseline. Pairwise statistics were calculated by Student's *t* tests.

Contextual fear conditioning test

The standard contextual fear conditioning test is conducted over 3 d. On the first day, which was the conditioning period, the mouse was placed in the conditioning chamber (Med Associates) for 3 min (phase A) before the onset of the sound at 2,800 Hz and 85 dB for 30 s (phase B, conditioning stimulus). The last 2 s of the conditioning stimulus was coupled with a 0.7-mA continuous foot shock (phase C, unconditioned stimulus). After resting an additional 30 s in the chamber, phases B and C were repeated once, and the mouse was returned to its home cage after resting in the chamber for 30 s On the second day, mice were tested for their contextual memory in the same chamber for 3 min without either sound or foot shock. On the third day, mice were tested for tone memory in a different chamber environment with the sound but no foot shock. Fear memory was measured as the percentage of freezing, which was defined as the percentage of time completely lacking movement, except for respiration, in intervals of 5 s.

Quantification of G-ratios

The myelinated axon circumference was measured by digitally tracing the inner and outer layers of the myelinated fiber

using ImageJ software. The G-ratio was calculated by dividing the inner circumference of the axon (without myelin) by the outer circumference of the total fiber (including myelin). Three pairs of BACE1$^{fl/fl/Nes\text{-}Cre}$ and BACE1$^{fl/fl}$ mice were processed for the quantification of G-ratios.

Statistical analysis

Statistical analysis was performed using Excel (Microsoft). All data values are expressed as mean ± SEM and were analyzed for statistical significance using an F–test for equal variance, followed by a two-tailed Student's *t* test. Significant p-values are denoted by the use of asterisks in the text and figures (*, $P < 0.05$; **, $P < 0.01$; ***, $P < 0.001$).

Online supplemental material

Fig. S1 shows the generation of BACE1$^{fl/fl}$ mice. Fig. S2 shows the expression of LacZ in broad brain regions in UbcCreER/R26R mice. Fig. S3 shows there are no significant alterations in myelination when BACE1 is deleted in the early adult. Fig. S4 shows there are no significant changes in astrogenesis or astrocytic hypertrophy in BACE1$^{fl/fl/UbcCreER}$ mouse brains. Fig. S5 shows increased microglial activation and dystrophic neurites correlates with amyloid plaque loads.

ACKNOWLEDGMENTS

We thank Dr. Chris Nelson for critical reading of this manuscript.

This study was supported by grants from the National Institutes of Health to R. Yan (NS074256, AG025493, AG046929, and NM103942).

The authors declare no competing financial interests.

Author contributions: X. Hu designed, conducted, acquired, and interpreted results, as well as participating in writing this paper. B. Das designed and performed electrophysiological experiments and data interpretation, as well as writing part of the paper. H. Hou and W. He performed some animal and biochemical experiments. R. Yan developed this project, interpreted data, and wrote the paper with input from all authors.

Submitted: 5 October 2017

Revised: 16 November 2017

Accepted: 4 January 2018

REFERENCES

Baba, A., T. Yasui, S. Fujisawa, R.X. Yamada, M.K. Yamada, N. Nishiyama, N. Matsuki, and Y. Ikegaya. 2003. Activity-evoked capacitative Ca2+ entry: implications in synaptic plasticity. *J. Neurosci.* 23:7737–7741.

Bach, M.E., R.D. Hawkins, M. Osman, E.R. Kandel, and M. Mayford. 1995. Impairment of spatial but not contextual memory in CaMKII mutant mice with a selective loss of hippocampal LTP in the range of the theta frequency. *Cell.* 81:905–915. https://doi.org/10.1016/0092-8674(95)90010-1

Barão, S., D. Moechars, S.F. Lichtenthaler, and B. De Strooper. 2016. BACE1 Physiological Functions May Limit Its Use as Therapeutic Target for Alzheimer's Disease. *Trends Neurosci.* 39:158–169. https://doi.org/10.1016/j.tins.2016.01.003

Ben Halima, S., S. Mishra, K.M.P. Raja, M. Willem, A. Baici, K. Simons, O. Brüstle, P. Koch, C. Haass, A. Caflisch, and L. Rajendran. 2016. Specific Inhibition of β-Secretase Processing of the Alzheimer Disease Amyloid Precursor Protein. *Cell Reports.* 14:2127–2141. https://doi.org/10.1016/j.celrep.2016.01.076

Braak, H., and E. Braak. 1997. Diagnostic criteria for neuropathologic assessment of Alzheimer's disease. *Neurobiol. Aging.* 18(4, Suppl):S85–S88. https://doi.org/10.1016/S0197-4580(97)00062-6

Cai, H., Y. Wang, D. McCarthy, H. Wen, D.R. Borchelt, D.L. Price, and P.C. Wong. 2001. BACE1 is the major beta-secretase for generation of Abeta peptides by neurons. *Nat. Neurosci.* 4:233–234. https://doi.org/10.1038/85064

Corriveau, R.A., W.J. Koroshetz, J.T. Gladman, S. Jeon, D. Babcock, D.A. Bennett, S.T. Carmichael, S.L. Dickinson, D.W. Dickson, M. Emr, et al. 2017. Alzheimer's Disease-Related Dementias Summit 2016: National research priorities. *Neurology.* 89:2381–2391. https://doi.org/10.1212/WNL.0000000000004717

Daria, A., A. Colombo, G. Llovera, H. Hampel, M. Willem, A. Liesz, C. Haass, and S. Tahirovic. 2017. Young microglia restore amyloid plaque clearance of aged microglia. *EMBO J.* 36:583–603. https://doi.org/10.15252/embj.201694591

De Strooper, B., T. Iwatsubo, and M.S. Wolfe. 2012. Presenilins and γ-secretase: structure, function, and role in Alzheimer Disease. *Cold Spring Harb. Perspect. Med.* 2:a006304. https://doi.org/10.1101/cshperspect.a006304

He, W., Y. Lu, I. Qahwash, X.Y. Hu, A. Chang, and R. Yan. 2004. Reticulon family members modulate BACE1 activity and amyloid-beta peptide generation. *Nat. Med.* 10:959–965. https://doi.org/10.1038/nm1088

Hu, X., Q. Shi, X. Zhou, W. He, H. Yi, X. Yin, M. Gearing, A. Levey, and R. Yan. 2007. Transgenic mice overexpressing reticulon 3 develop neuritic abnormalities. *EMBO J.* 26:2755–2767. https://doi.org/10.1038/sj.emboj.7601707

Hu, X., Q. Fan, H. Hou, and R. Yan. 2016. Neurological dysfunctions associated with altered BACE1-dependent Neuregulin-1 signaling. *J. Neurochem.* 136:234–249. https://doi.org/10.1111/jnc.13395

Hussain, I., D. Powell, D.R. Howlett, D.G. Tew, T.D. Meek, C. Chapman, I.S. Gloger, K.E. Murphy, C.D. Southan, D.M. Ryan, et al. 1999. Identification of a novel aspartic protease (Asp 2) as beta-secretase. *Mol. Cell. Neurosci.* 14:419–427. https://doi.org/10.1006/mcne.1999.0811

Itoh, K., K. Shimono, and V. Lemmon. 2005. Dephosphorylation and internalization of cell adhesion molecule L1 induced by theta burst stimulation in rat hippocampus. *Mol. Cell. Neurosci.* 29:245–249. https://doi.org/10.1016/j.mcn.2005.02.014

Jonsson, T., J.K. Atwal, S. Steinberg, J. Snaedal, P.V. Jonsson, S. Bjornsson, H. Stefansson, P. Sulem, D. Gudbjartsson, J. Maloney, et al. 2012. A mutation in APP protects against Alzheimer's disease and age-related cognitive decline. *Nature.* 488:96–99. https://doi.org/10.1038/nature11283

Kim, S., Y. Sato, P.S. Mohan, C. Peterhoff, A. Pensalfini, A. Rigoglioso, Y. Jiang, and R.A. Nixon. 2016. Evidence that the rab5 effector APPL1 mediates APP-βCTF-induced dysfunction of endosomes in Down syndrome and Alzheimer's disease. *Mol. Psychiatry.* 21:707–716. https://doi.org/10.1038/mp.2015.97

Lauritzen, I., R. Pardossi-Piquard, A. Bourgeois, S. Pagnotta, M.G. Biferi, M. Barkats, P. Lacor, W. Klein, C. Bauer, and F. Checler. 2016. Intraneuronal aggregation of the β-CTF fragment of APP (C99) induces Aβ-independent lysosomal-autophagic pathology. *Acta Neuropathol.* 132:257–276. https://doi.org/10.1007/s00401-016-1577-6

Lin, X., G. Koelsch, S. Wu, D. Downs, A. Dashti, and J. Tang. 2000. Human aspartic protease memapsin 2 cleaves the beta-secretase site of beta-amyloid precursor protein. *Proc. Natl. Acad. Sci. USA.* 97:1456–1460. https://doi.org/10.1073/pnas.97.4.1456

Luo, Y., B. Bolon, S. Kahn, B.D. Bennett, S. Babu-Khan, P. Denis, W. Fan, H. Kha, J. Zhang, Y. Gong, et al. 2001. Mice deficient in BACE1, the Alzheimer's beta-secretase, have normal phenotype and abolished beta-amyloid generation. *Nat. Neurosci.* 4:231–232. https://doi.org/10.1038/85059

Malenka, R.C., and R. Malinow. 2011. Alzheimer's disease: Recollection of lost memories. *Nature.* 469:44–45. https://doi.org/10.1038/469044a

Mei, L., and K.A. Nave. 2014. Neuregulin-ERBB signaling in the nervous system and neuropsychiatric diseases. *Neuron*. 83:27–49. https://doi.org/10.1016/j.neuron.2014.06.007

Mullan, M., F. Crawford, K. Axelman, H. Houlden, L. Lilius, B. Winblad, and L. Lannfelt. 1992. A pathogenic mutation for probable Alzheimer's disease in the APP gene at the N-terminus of beta-amyloid. *Nat. Genet.* 1:345–347. https://doi.org/10.1038/ng0892-345

Oakley, H., S.L. Cole, S. Logan, E. Maus, P. Shao, J. Craft, A. Guillozet-Bongaarts, M. Ohno, J. Disterhoft, L. Van Eldik, et al. 2006. Intraneuronal beta-amyloid aggregates, neurodegeneration, and neuron loss in transgenic mice with five familial Alzheimer's disease mutations: potential factors in amyloid plaque formation. *J. Neurosci.* 26:10129–10140. https://doi.org/10.1523/JNEUROSCI.1202-06.2006

Roberds, S.L., J. Anderson, G. Basi, M.J. Bienkowski, D.G. Branstetter, K.S. Chen, S.B. Freedman, N.L. Frigon, D. Games, K. Hu, et al. 2001. BACE knockout mice are healthy despite lacking the primary beta-secretase activity in brain: implications for Alzheimer's disease therapeutics. *Hum. Mol. Genet.* 10:1317–1324. https://doi.org/10.1093/hmg/10.12.1317

Ruzankina, Y., C. Pinzon-Guzman, A. Asare, T. Ong, L. Pontano, G. Cotsarelis, V.P. Zediak, M. Velez, A. Bhandoola, and E.J. Brown. 2007. Deletion of the developmentally essential gene ATR in adult mice leads to age-related phenotypes and stem cell loss. *Cell Stem Cell.* 1:113–126. https://doi.org/10.1016/j.stem.2007.03.002

Sadleir, K.R., W.A. Eimer, S.L. Cole, and R. Vassar. 2015. Aβ reduction in BACE1 heterozygous null 5XFAD mice is associated with transgenic APP level. *Mol. Neurodegener.* 10:1. https://doi.org/10.1186/1750-1326-10-1

Selkoe, D.J., and J. Hardy. 2016. The amyloid hypothesis of Alzheimer's disease at 25 years. *EMBO Mol. Med.* 8:595–608. https://doi.org/10.15252/emmm.201606210

Sharoar, M.G., Q. Shi, Y. Ge, W. He, X. Hu, G. Perry, X. Zhu, and R. Yan. 2016. Dysfunctional tubular endoplasmic reticulum constitutes a pathological feature of Alzheimer's disease. *Mol. Psychiatry.* 21:1263–1271. https://doi.org/10.1038/mp.2015.181

Shi, Q., Y. Ge, M.G. Sharoar, W. He, R. Xiang, Z. Zhang, X. Hu, and R. Yan. 2014. Impact of RTN3 deficiency on expression of BACE1 and amyloid deposition. *J. Neurosci.* 34:13954–13962. https://doi.org/10.1523/JNEUROSCI.1588-14.2014

Shimono, K., D. Kubota, F. Brucher, M. Taketani, and G. Lynch. 2002. Asymmetrical distribution of the Schaffer projections within the apical dendrites of hippocampal field CA1. *Brain Res.* 950:279–287. https://doi.org/10.1016/S0006-8993(02)03052-4

Sinha, S., J.P. Anderson, R. Barbour, G.S. Basi, R. Caccavello, D. Davis, M. Doan, H.F. Dovey, N. Frigon, J. Hong, et al. 1999. Purification and cloning of amyloid precursor protein beta-secretase from human brain. *Nature.* 402:537–540. https://doi.org/10.1038/990114

Sisodia, S.S., and P.H. St George-Hyslop. 2002. gamma-Secretase, Notch, Abeta and Alzheimer's disease: where do the presenilins fit in? *Nat. Rev. Neurosci.* 3:281–290. https://doi.org/10.1038/nrn785

Tamayev, R., S. Matsuda, O. Arancio, and L. D'Adamio. 2012. β- but not γ-secretase proteolysis of APP causes synaptic and memory deficits in a mouse model of dementia. *EMBO Mol. Med.* 4:171–179. https://doi.org/10.1002/emmm.201100195

Vassar, R. 2014. BACE1 inhibitor drugs in clinical trials for Alzheimer's disease. *Alzheimers Res. Ther.* 6:89. https://doi.org/10.1186/s13195-014-0089-7

Vassar, R., B.D. Bennett, S. Babu-Khan, S. Kahn, E.A. Mendiaz, P. Denis, D.B. Teplow, S. Ross, P. Amarante, R. Loeloff, et al. 1999. Beta-secretase cleavage of Alzheimer's amyloid precursor protein by the transmembrane aspartic protease BACE. *Science.* 286:735–741. https://doi.org/10.1126/science.286.5440.735

Vassar, R., P.H. Kuhn, C. Haass, M.E. Kennedy, L. Rajendran, P.C. Wong, and S.F. Lichtenthaler. 2014. Function, therapeutic potential and cell biology of BACE proteases: current status and future prospects. *J. Neurochem.* 130:4–28. https://doi.org/10.1111/jnc.12715

Yan, R. 2016. Stepping closer to treating Alzheimer's disease patients with BACE1 inhibitor drugs. *Transl. Neurodegener.* 5:13. https://doi.org/10.1186/s40035-016-0061-5

Yan, R. 2017. Physiological Functions of the β-Site Amyloid Precursor Protein Cleaving Enzyme 1 and 2. *Front. Mol. Neurosci.* 10:97. https://doi.org/10.3389/fnmol.2017.00097

Yan, R., and R. Vassar. 2014. Targeting the β secretase BACE1 for Alzheimer's disease therapy. *Lancet Neurol.* 13:319–329. https://doi.org/10.1016/S1474-4422(13)70276-X

Yan, R., M.J. Bienkowski, M.E. Shuck, H. Miao, M.C. Tory, A.M. Pauley, J.R. Brashier, N.C. Stratman, W.R. Mathews, A.E. Buhl, et al. 1999. Membrane-anchored aspartyl protease with Alzheimer's disease beta-secretase activity. *Nature.* 402:533–537. https://doi.org/10.1038/990107

Yan, R., Q. Fan, J. Zhou, and R. Vassar. 2016. Inhibiting BACE1 to reverse synaptic dysfunctions in Alzheimer's disease. *Neurosci. Biobehav. Rev.* 65:326–340. https://doi.org/10.1016/j.neubiorev.2016.03.025